Electronic Supplementary Material (ESI) for Nanoscale.

Supporting Information

Vertically-oriented MoS_2 nanosheets for nonlinear optical devices

M. Bolhuis[1], J. Hernandez-Rueda[1], S. E. van Heijst[1], M. Tinoco Rivas[1,†], L. Kuipers[1], and S. Conesa-Boj[1,]*

[1] Kavli Institute of Nanoscience, Delft University of Technology, 2628CJ Delft, The Netherlands

*E-mail: s.conesaboj@tudelft.nl

A. Synthesis of vertically-oriented MoS_2 nanosheets.

Figure S1 provides a schematic illustration of the growth protocol adopted for the growth of the vertically-oriented MoS_2 nanosheets. Before the sulfurization, a pre-treatment with Ar flow (500 sccm) during 30 min was carried out. This pre-treatment was followed by a gradually ramp up of the temperature at a rate of 10 °C /min. The temperature of zone 2, were the wafer containing the Mo seed layer was placed, was ramped up to the desired reaction temperature in the range between 500 °C and 700 °C. We note that the Ar gas flow was reduced from 500 sccm down to 150 sccm once the temperature in zone 2 reached 500 °C.

Once the temperature of zone 2 reached the target reaction temperature, we started to ramp up the temperature in zone 3, were the Sulfur powder was located, up to 220 °C at a rate of 10 °C /min. We defined the initial reaction time as the time when the temperature of the Sulfur reached 220 °C, and from this point onwards we measured the total reaction time of the Sulfur with the Mo seed layer. Once the desired reaction time was reached, the heating of both zones of the furnace was switched off at the same time. While the furnace tube cooled down to room temperature, the Ar gas flow was kept running.

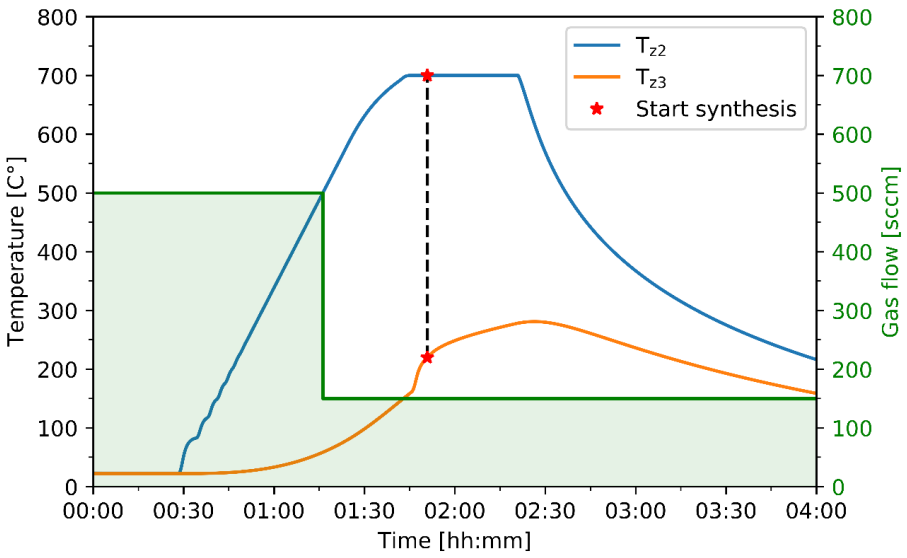

Figure S1. Schematic illustration of the growth protocol adopted for the growth of vertically-oriented MoS_2 nanosheets. We display the temperature (left *y*-axis) and the Ar gas flow (right *y*-axis) as a function of the reaction time. In this scheme, T_{z2} and T_{z3} indicate the temperatures of zones 2 and 3 of the furnace respectively. The stars indicate the points defined as the starting times of the reaction.

Argon flow dependence. – **Figure S2** displays the variation of the MoS_2 thickness as the Ar flow rate is increased. We found that as the Ar flow rate increased, the MoS_2 thickness increased as well until a maximum value of about 1μm at an Ar flow rate of 75 sccm was reached. From this point onwards, the MoS_2 thickness instead decreased with further increases of the Ar flow rate. For this reason, in the design of the growth parameters, we only considered Ar flow rates above 75 sccm, for which the expected trend that higher flow rates slow the reaction and lead to thinner MoS_2 was verified. Specifically, for all the experiments presented in this work we fixed the Ar flow at a value of 150 sccm.[1]

[1] Kong, D.; et al. Synthesis of MoS_2 and $MoSe_2$ films with Vertically Aligned Layers. *Nano Lett.* **2013**, 13, 1341.

It is worth mentioning that the growth of v-MoS_2 nanosheets via sulfurization can be strongly dependent on the Ar flow when the furnace tube is affected by flow instabilities. In **Figure S2** we also display two points (red crosses) corresponding to growths affected by such instabilities in the tube furnace. The results of these growths differed significantly from the main trend, and thus were not considered further.

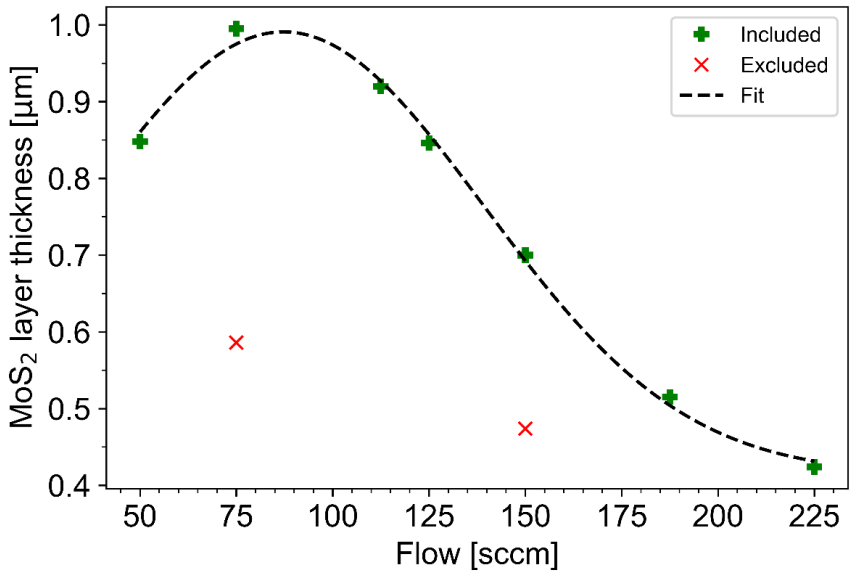

Figure 2S. The thickness of the grown MoS_2 layer as a function of the Ar gas flow. The model fit is based on the data points labelled with a green cross. We observe that for Ar flows above 75 sccm the MoS_2 thickness decreases monotonically as the flow is increased.

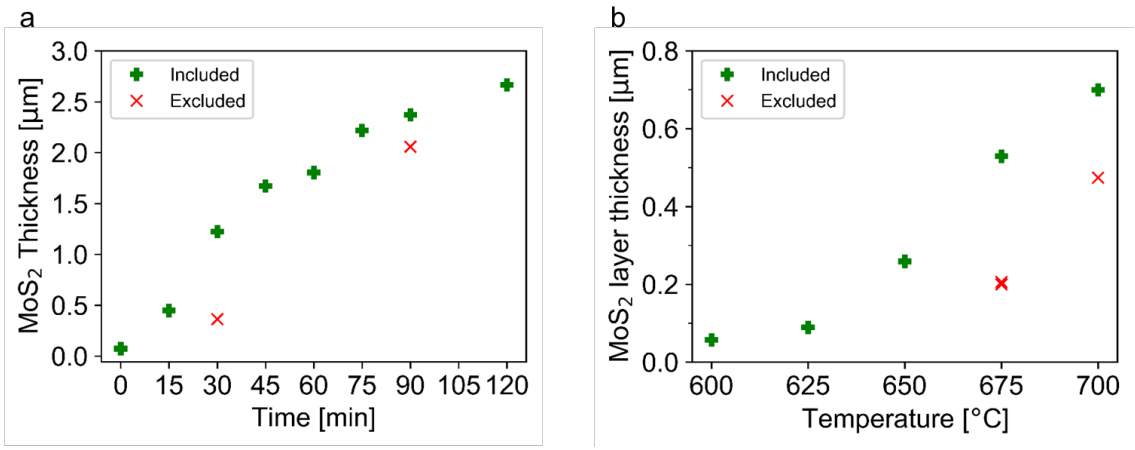

Figure 3S. Same as **Figure 2S** with the resulting MoS_2 thicknesses represented as a function of the reaction time (**3a**) and of the reaction temperature (**3b**).

In **Figures S3a** and **S3b** we display the results corresponding to the same growths reported in **Figure S2** now with the resulting MoS_2 thicknesses being represented as a function of the reaction time and the reaction temperature respectively. From this comparison one also observes that, while most of the data points follow the expected clear trend, the presence of instabilities in the tube furnace related to the Ar gas flow can result in significant variations in the growth rate.

B. Structural characterization of v-MoS_2 nanosheets.

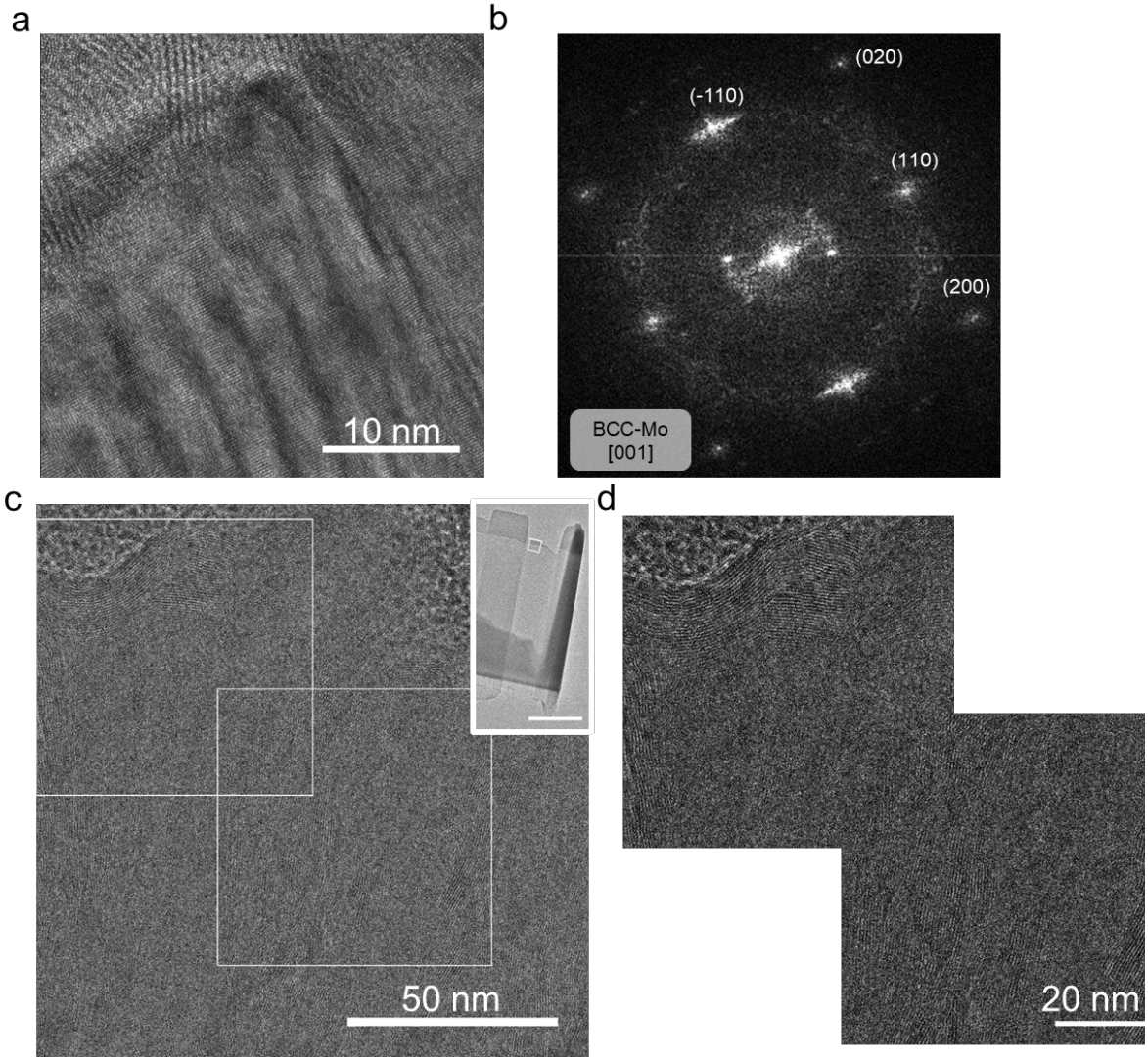

Figure S4. (a) and **(b)** HRTEM image taken from a representative specimen sulfurized at 700 °C displaying a region of the Mo-metal seed layer and the corresponding FFT, indicating that the Mo is characterized by the BCC crystal phase. **(c)** HRTEM image of the upper region of the grown MoS_2 (see inset) immediately below the Pt protective layer. In **(d)** we show the inverse FFT calculated from the two regions marked with white squares in **(c).**

Figure S4 displays a cross section HRTEM analysis of one of the representative specimens sulfurized at a temperature of 700 °C. Measurements were taken at different regions of the cross-section lamella: at the Mo seed layer (**Figure S4a**), at the interface between the Mo seed layer and the v-MoS_2 nanosheets (**Figure S4c**), and at the first nanometers from the surface of the sulfurized lamella (**Figure S4d**)**.** In the first case, we also include the corresponding FFT indicating that the Mo-metal crystallizes in the BCC structure. In the latter case, the MoS_2 nanosheets were found to exhibit random orientations: in the first 20 nm from the surface (beneath the Pt protective layer), vertical and horizontal nanosheets appear simultaneously, as can be seen from the orientations of lattice fringes in **Figure S4d**. Afterwards, the rest of the grown MoS_2 is restricted to the vertical orientation.

Different scenarios have been proposed to explain the appearance of a orientation-disordered region where both horizontal and vertical MoS_2 are present. Our experimental findings are consistent with the theoretical modelling of the diffusion-reaction growth proposed for the synthesis of vertically-oriented MoS_2.[2] This model describes the v-MoS_2 growth from the co-existence of two different morphologies, the first an orientation-disordered region extending from the surface to the first few nanometers, and the region containing exclusively vertically-oriented MoS_2 nanosheets.

[2] Stern, C. et al. Growth Mechanism and Electronic Properties of Vertically-aligned MoS_2. *Scientific Reports* **2018**, 8,16480.

C. Chemical analysis of the cross-section TEM lamellas the v-MoS_2 nanosheets.

A Python analysis code was developed and used to process and interpret the EDX line spectra data. In the following we describe how the S/Mo atomic ratio was calculated at three different locations of the chemical spectra. **Figure S5a** displays the elemental atomic percentage profile taken along the cross-section lamella, from the protective layer Pt (violet line) to the Silicon wafer (red line). **Figure S5b** then shows the same raw data after applying a Savitzky-Golay filter in order to smoothen the stochastic fluctuations. **Figure S5c** represents the data restricted to the points that we defined as top and bottom of the MoS_2 sulfurized region. We determined the cross-point between the Pt and S (from the top) and between the S and Mo (in the bottom), and then we chose three different locations to automatically calculate the S/Mo ratio. We selected these three locations at distances of 35% (close to the surface), 50%, and 65% respectively. All the calculated S/Mo ratios were then collected and plotted in **Figure S5e.** From this figure, we can observe that for times below 15 min the sulfurization is not fully complete. From the same plot we can also observe that the S/Mo ratio remains stable along the lamella.

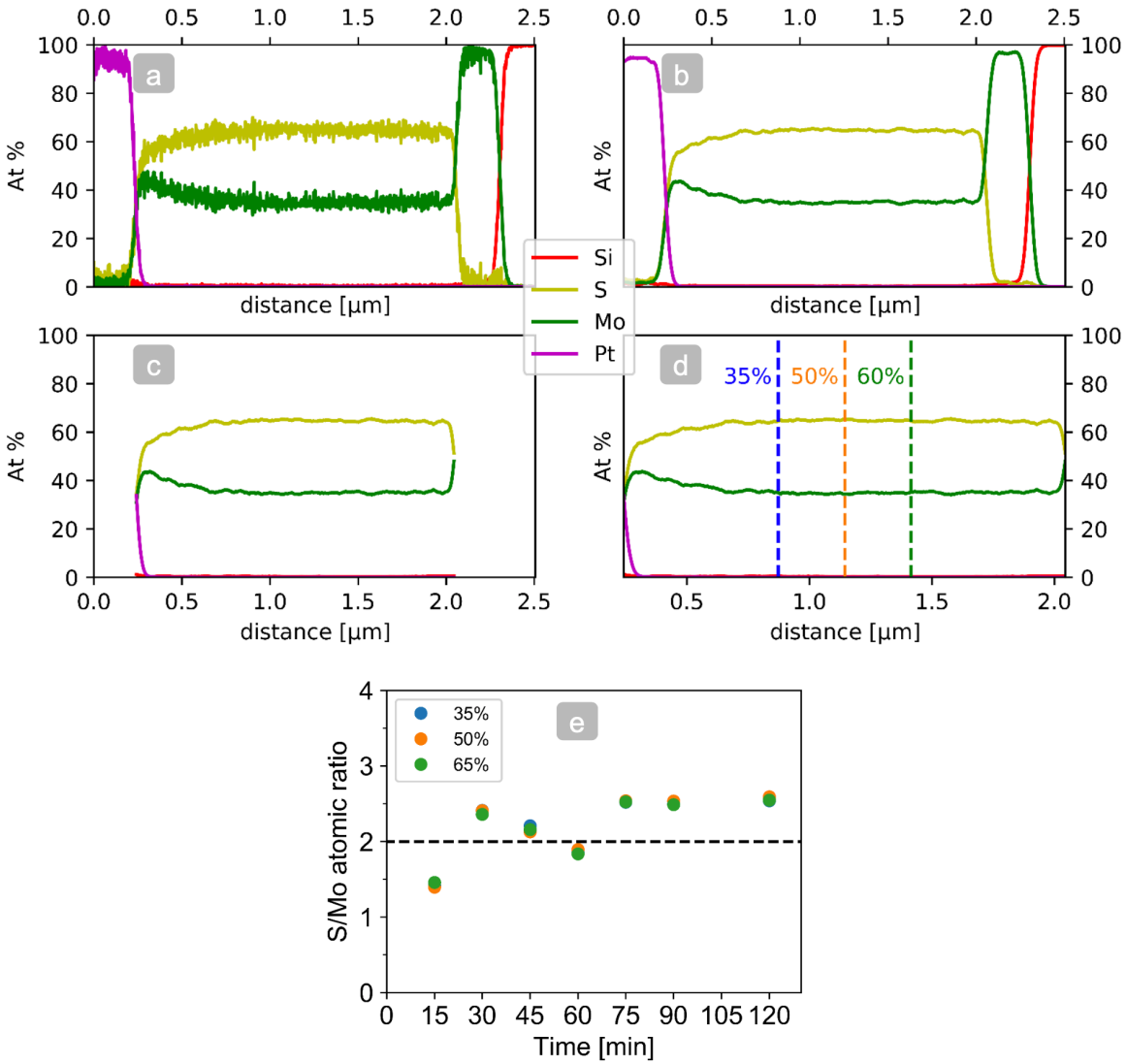

Figure S5. **(a)** The elemental atomic percentage profile taken along the cross-section lamella, from the protective layer Pt (violet line) to the Silicon wafer (red line). **(b)** Same raw data after applying a Savitzky-Golay filter in order to smoothen the stochastic fluctuations. **(c)** The same data now restricted to the points defined as the top and bottom of the MoS_2 sulfurized region. **(d)** The three different locations selected to calculate the S/Mo ratio, see text. **(e)** Summary of the calculated S/Mo ratios calculated as a function of the reaction time.

D. Raman spectroscopy of exfoliated MoS_2 flakes.

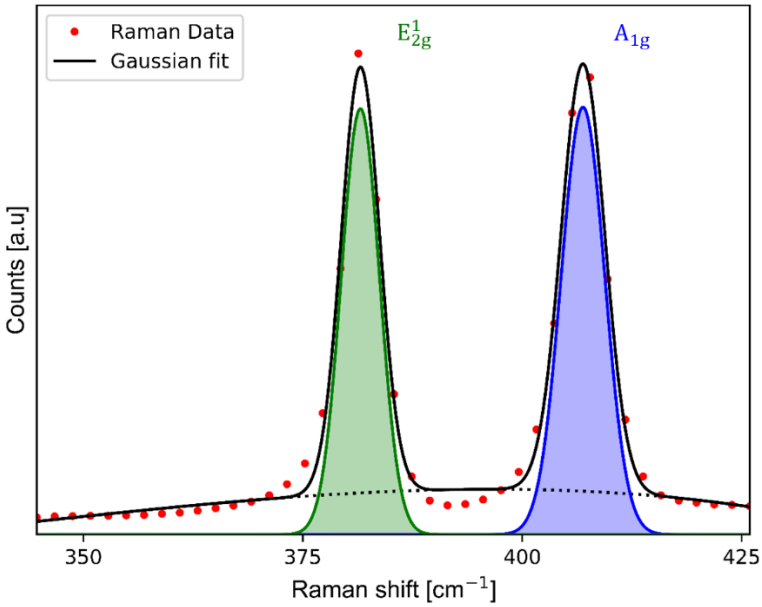

Figure S6. Raman emission spectra taken on a regular exfoliated MoS_2 flake using the same experimental set-up as in **Figures 1c** and **1d** in the main manuscript. We observe that the intensity of the two dominating Raman modes, E^1_{2g} and A_{1g}, is very similar and therefore the ratio of intensities is close to unity. These two Raman peaks are associated to the in-plane and out-of-plane vibration modes respectively.

E. Sample preparation for nonlinear optical measurements.

Horizontally-oriented MoS_2 sample preparation. – The horizontal MoS_2 flakes were directly grown onto a Si_3N_4 TEM grid. A vapor-solid growth mechanism was used. The Si_3N_4 TEM grid was placed next to a Mo-seed layer in the middle zone of the tube furnace, with the sulfur located upstream from the sample. From this step onwards, the rest of the growth process is the same as the one described in **A**.

Vertically-oriented MoS_2 sample preparation. – The vertical MoS_2 specimen was prepared using the ultramicrotomy technique.[3] This method allows us to prepare the specimen ensuring that a large area is available both for TEM inspection and for nonlinear optical measurements.

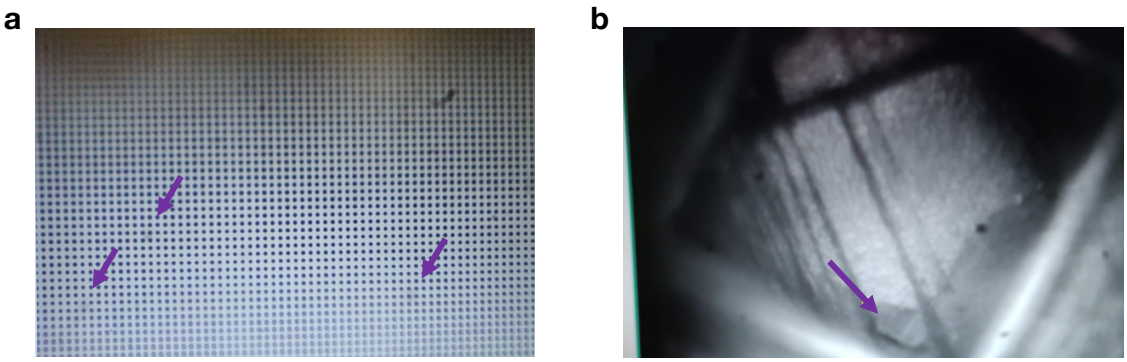

Figure S7. (a) and **(b)** low magnification optical images of the two TEM grids containing the horizontal and vertical MoS_2 nanosheets, respectively. We indicate with arrows the location of some of the MoS_2 specimens.

[3] M. O. Cichocka, et al. Robust Sample Preparation of Large-Area In- and Out-of-Plane Cross Sections of Layered Materials with Ultramicrotomy, *ACS Appl. Mater. Interfaces* **2020**, 12, 15867.

F. Nonlinear response of a MoS_2 sample.

To calibrate our experimental multi-photon spectroscopy system, we studied the nonlinear response of a MoS_2 sample and thin nanostructured gold samples.[4] **Figure S8** illustrates several nonlinear signals as a function of the laser energy. The solid lines display fits to monomial functions. The fits to the four-wave mixing signal illustrate a linear and quadratic behavior with the energy of the laser at ω_2 and ω_1 (*i.e.* $\omega_{FWM} = 2\omega_1 - \omega_2$). The fits to the third harmonic generation signal originated from the interaction of the laser at ω_2 and the sample follows a cubic response (*i.e.* $\omega_{TGH} = 3\omega_2$). The laser energy dependencies observed here are consistent with the equations of the polarization vector.[5]

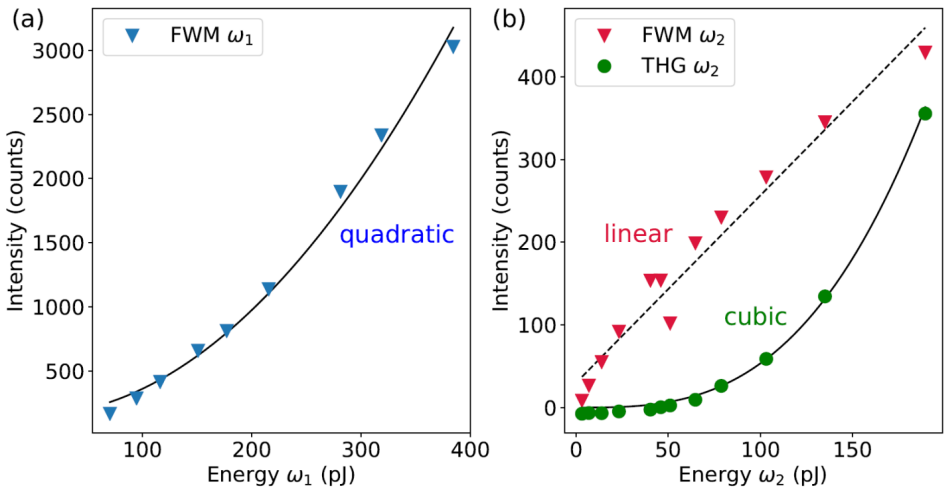

Figure S8. (a) FWM signal as a function of the laser energy per pulse at ω_1. **(b)** FWM and THG signals as a function of the laser energy per pulse at ω_2. The energies of the beams at ω_1 in **(b)** and ω_2 in **(a)** correspond to 56 pJ and 51 pJ at a repetition rate of 80 MHz and with a pulse duration of approximately 230 fs. The solid lines are fits to monomial functions of first, second and third order.

[4] M.L. Noordam, et. al. Plasmon-induced enhancement of nonlinear optical processes in a double-resonant metallic nanostructure grating, *Applied Physics Letters* **2020**, 116, 101101.

[5] Boyd, R. W. Nonlinear optics. Elsevier, **2013**

G. Nonlinear response of a MoS_2 sample.

In the main text we discuss the ratio of the second-order nonlinear susceptibilities of the vertical $\chi_V^{(2)}$ and horizontally $\chi_H^{(2)}$ oriented flakes of MoS_2. Here, we detail the formulae of the second-order polarization vector $P^{(2)}$ for SHG and SFG used for the calculation of the ratios. These can also be found in Nonlinear Optics by R. Boyd.[6]

$$P_{SHG}^{(2)} = \chi^{(2)} E_2 E_2 \rightarrow \chi^{(2)} \propto \sqrt{I_{SHG}/I_2 I_2}$$

$$P_{SFG}^{(2)} = \chi^{(2)} E_1 E_2 \rightarrow \chi^{(2)} \propto \sqrt{I_{SFG}/I_1 I_2}$$

where E_1 and E_2 are the electric field strength of the laser at 776 nm and 1210 nm, respectively and I_1 and I_2 are the intensities of the laser. By using the experimental laser parameters combined with the spectral peaks presented in the spectra, we can therefore obtain the ratios of the second-order susceptibilities both using SHG and SFG signals:

$$\left.\frac{\chi_V^{(2)}}{\chi_H^{(2)}}\right]_{SHG} = \frac{\sqrt{I_{SHG}^V / I_2^V I_2^V}}{\sqrt{I_{SHG}^H / I_2^H I_2^H}}$$

$$\left.\frac{\chi_V^{(2)}}{\chi_H^{(2)}}\right]_{SFG} = \frac{\sqrt{I_{SFG}^V / I_1^V I_2^V}}{\sqrt{I_{SFG}^H / I_1^H I_2^H}}$$

We note that considering that the MoS_2 layer thickness is smaller than the optical penetration depth and the coherence length of the laser, we neglect both absorption and phase matching effects in our estimation of the nonlinear susceptibility.[7,8]

---

[6] Boyd, R. W. Nonlinear optics. Elsevier, **2013.**

[7] R. Wang et al. Third-harmonic generation in ultrathin films of MoS_2, *ACS Appl. Mater. Interfaces* **2014**, 6, 314-318.

[8] N. Kumar et al. Second harmonic microscopy of monolayer MoS_2, *Phys. Rev. B* **2013,** 87, 161403.